Article

Oxidation Mechanism of Aromatic Peroxy and Bicyclic Radicals from OH–Toluene Reactions

Inseon Suh, Renyi Zhang, Luisa T. Molina, and Mario J. Molina

J. Am. Chem. Soc., **2003**, 125 (41), 12655-12665• DOI: 10.1021/ja0350280 • Publication Date (Web): 19 September 2003

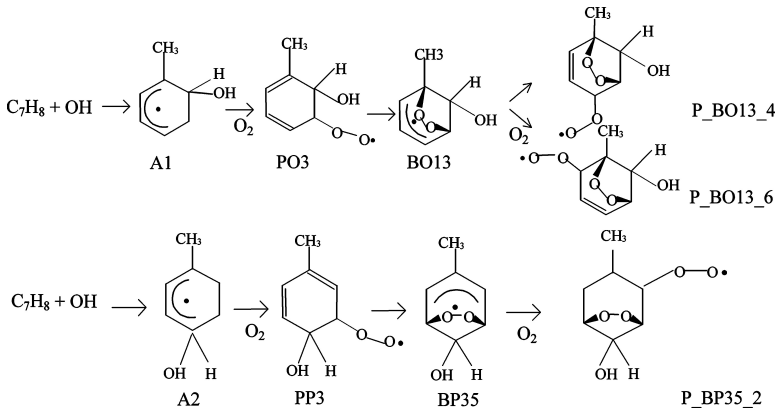

More About This Article

Additional resources and features associated with this article are available within the HTML version:

- Supporting Information
- Links to the 9 articles that cite this article, as of the time of this article download
- Access to high resolution figures
- Links to articles and content related to this article
- Copyright permission to reproduce figures and/or text from this article

View the Full Text HTML

J|A|C|S
ARTICLES
Published on Web 09/19/2003

Oxidation Mechanism of Aromatic Peroxy and Bicyclic Radicals from OH−Toluene Reactions

Inseon Suh,[†] Renyi Zhang,*[,†] Luisa T. Molina,[§] and Mario J. Molina[§]

Contribution from the Department of Atmospheric Sciences, Texas A&M University, College Station, Texas 77843, and the Departments of Earth, Atmospheric, and Planetary Sciences and Chemistry, Massachusetts Institute of Technology, Cambridge, Massachusetts 02139

Received March 6, 2003; E-mail: zhang@ariel.met.tamu.edu

Abstract: Theoretical calculations have been performed to investigate mechanistic features of OH-initiated oxidation reactions of toluene. Aromatic peroxy radicals arising from initial OH and subsequent O_2 additions to the toluene ring are shown to cyclize to form bicyclic radicals rather than undergoing reaction with NO under atmospheric conditions. Isomerization of bicyclic radicals to more stable epoxide radicals possesses significantly higher barriers and, hence, has slower rates than O_2 addition to form bicyclic peroxy radicals. At each OH attachment site, only one isomeric pathway via the bicyclic peroxy radical is accessible to lead to ring cleavage. The study provides thermochemical and kinetic data for quantitative assessment of the photochemical production potential of ozone and formation of toxic products and secondary organic aerosol from toluene oxidation.

Introduction

Aromatic hydrocarbons constitute an important fraction (∼20%) of total volatile organic compounds (VOCs) in the urban atmosphere and play a major role in urban air pollution.[1−3] Emissions of aromatic hydrocarbons are primarily from anthropogenic sources, i.e., emission from automobiles, fuel-based vehicles, and industry.[3] In addition to their important role in photochemical ozone production, oxidation of aromatic hydrocarbons leads to formation of nonvolatile and semi-volatile organic compounds, which are responsible for secondary organic aerosol (SOA) formation.[3−5] The SOA may impact human health and the climate.[3] Also, the likely formation of toxic epoxide products from aromatic oxidation is of considerable concern.[6] Because the epoxy functional group can serve as an electrophile to attack DNA and nucleosides, epoxides have been considered for their carcinogenic and mutagenic properties.[7,8]

Toluene is the most abundant aromatic hydrocarbon in the atmosphere. Photochemical oxidation of toluene is mainly initiated by attack from hydroxyl radical OH. The OH−toluene reaction results in minor H-atom abstraction from the methyl group and major OH addition to the aromatic ring (about 90%).[1−3] Under atmospheric conditions, the OH−toluene adduct reacts with O_2 either by O_2 addition to form (primary) peroxy radicals or by H-abstraction to yield phenolic compounds. The latter channel has been shown to be relatively minor, accounting for about 16% of the total products. The fate of the peroxy radicals is governed by competition between reaction with NO to form alkoxy radicals and cyclization to form bicyclic radicals. The bicyclic radicals can undergo unimolecular rearrangement to form epoxide radicals or bimolecular reaction with O_2 to form (secondary) bicyclic peroxy radicals. The mechanistic complexity of the toluene oxidation further arises from multiple isomeric pathways at each reaction stage. Initial OH addition to toluene results in four distinct structural OH−toluene adduct isomers (i.e., ortho, para, ispo, and meta) (A1−A4). Subsequent reactions of OH−toluene adducts with O_2 and cyclization of aromatic peroxy radicals also incur additional isomeric branching.[9] Schemes 1 and 2 illustrate the likely pathways of toluene oxidation following OH addition to the ortho and para positions, respectively. For the ortho OH−toluene adduct, for example, O_2 addition to the aromatic ring occurs at C1, C3, or C5 on the ring, forming three possible structural isomers of the peroxy radicals. The next step involves formation of bicyclic radicals with an O−O bridge across the benzene ring, forming five possible isomers. The bicyclic radicals may isomerize to form eight possible epoxide radicals.

There has been considerable experimental and theoretical work on the OH-initiated reactions of toluene. Experimental studies have investigated the temperature- and pressure-dependent rate constant of the initial OH−toluene reaction,[10−12] and in particular, recent experimental work has been carried out to

[†] Texas A&M University.
[§] Massachusetts Institute of Technology.

(1) Calvert, J. G.; Atkinson, R.; Becker, K. H.; Kamens, R. M.; Seinfeld, J. H.; Wallington, T. J.; Yarwood, G. *The Mechanisms of Atmospheric Oxidation of Aromatic Hydrocarbons*; Oxford University Press: New York, 2002.
(2) Atkinson, R. *J. Phys. Chem. Ref. Data* **1997**, *26*, 215.
(3) Seinfeld, J. H.; Pandis, S. N. *Atmospheric Chemistry and Physics: From Air Pollution to Climate Change*; John Wiley & Sons: New York, 1997.
(4) Odum, J. R.; Jungkamp, T. P. W.; Griffin, R. J.; Flagan, R. C.; Seinfeld, J. H. *Science* **1997**, *96*, 276.
(5) Forstner, H. J. L.; Flagan, R. C.; Seinfeld, J. H. *Environ. Sci. Technol.* **1997**, *31*, 1345.
(6) Yu, J.; Jeffries, H. E. *Atmos. Environ.* **1997**, *31*, 2281.
(7) Ehrenberg, L.; Hussain, S. *Mutat. Res.* **1981**, *86*, 1.
(8) Hemminki, K. *Arch. Toxicol.* **1983**, *52*, 249.
(9) Garcia-Cruz, I.; Castro, M.; Vivier-Bunge, A. *J. Comput. Chem.* **2000**, *21*, 716.

Scheme 1

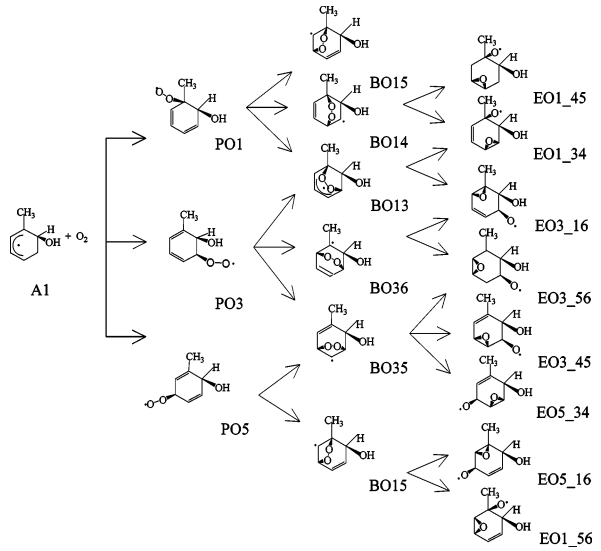

Scheme 2

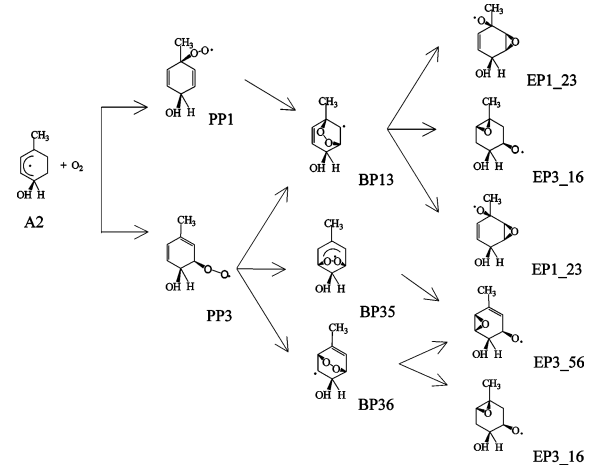

detect the intermediate radicals from the OH−toluene reactions.[11,12] Environmental chamber studies have also identified several major products consisting of both ring-retaining and fragmentation compounds.[4−6,13,14] In the presence of O_2 and NO_x, the identified reaction products include hydroxyl aromatic compounds, 2-, 4-, and 3-NO_2−toluene, along with ring cleavage products such as glyoxal, methylglyoxal, and butenedial. The most abundant hydroxyl aromatic compound has been identified as *o*-cresol.[13] A recent experimental study reported a significant yield (about 40 ± 10%) of glyoxal and indicated that the ring-cleavage pathway involving the bicyclic peroxy radical represents the major pathway in the oxidation of monocyclic aromatic hydrocarbons.[14] In addition, it has been suggested that the major SOA components comprise unsaturated anhydrides resulting from ring cleavage.[4,5]

Several theoretical studies have been performed to investigate the structures and energetics of the intermediate radicals from the OH-initiated oxidation of toluene, providing further insight into the mechanism of the OH−toluene reactions.[9,15−18]

At present, however, the detailed mechanism of toluene oxidation remains highly speculative. Most of the aromatic intermediate radicals have not yet been detected directly in the gas phase.[11,12] In previous experimental product studies, the carbon balance is less than 50%.[1−3] Even in situations where compounds have been identified as significant reaction products (for instance, in the cases of glyoxal and methyl glyoxal), unique routes leading to their formation have not been unambiguously established. Interpretation of the identified reaction products is primarily hindered because of the existence of multiple reaction pathways and steps.

In this work, we report a theoretical study of the aromatic peroxy, bicyclic, epoxide, and bicyclic peroxy radicals from the OH−toluene reactions. Reaction energies for the formation of the aromatic radicals were obtained to determine their relative stability and reversibility, and activation barriers were analyzed to assess the energetically favorable pathways to propagate the toluene oxidation. Kinetic calculations were performed using the classic transition state theory (TST) and RRKM/master equation to assess the atmospheric degradation mechanism of the OH−toluene reaction system. Relevance of the present theoretical work to interpretation of available experimental product studies was emphasized.

Theoretical Method

The quantum chemical computations were carried out similarly to those in our previous work.[18] Briefly, the theoretical calculations were performed on an SGI Origin 3800 supercomputer using the Gaussian 98 software package.[19] All radicals were treated with the unrestricted Hartree−Fock (UHF) formulation. Geometry optimization was executed using Becke's three-parameter hybrid method employing the LYP correction function (B3LYP) in conjunction with the split valence polarized basis set 6-31G(d,p). The DFT structures were then employed in single-point energy calculations using frozen-core second-order Møller−Plesset perturbation theory (MP2) and coupled-cluster theory with single and double excitations including perturbative corrections for the triple excitations (CCSD(T)) with various basis sets. Harmonic vibrational frequency calculations were performed using B3LYP/6-31G-(d,p). We corrected basis set effects on the calculated energies of the OH−toluene intermediate radicals, on the basis of an approach that was developed and validated to obtain the energetics of several addition

(10) (a) Knispel, R.; Koch, R.; Siese, M.; Zetzsch, C. *Ber. Bunsen-Ges. Phys. Chem.* **1990**, *94*, 1375. (b) Perry, R. A.; Atkinson, R.; Pitts, J. N.; *J. Phys. Chem.* **1997**, *81*, 296. (c) Bourmada, N.; Devolder, P.; Sochet, L. R. *Chem. Phys. Lett.* **1988**, *149*, 339.
(11) Molina, M. J.; Zhang, R.; Broekhuizen, K.; Lei, W.; Navarro, R.; Molina, L. T. *J. Am. Chem. Soc.* **1999**, *212*, 10225.
(12) Bohn, B. *J. Phys. Chem.* **2001**, *105*, 6092.
(13) (a) Shepson, P. B.; Edney, E. O.; Corse, E. W. *J. Phys. Chem.* **1984**, *88*, 4122. (b) Lonneman, W. A.; Seila, R. L.; Bufaline, J. J. *Environ. Sci. Tech.* **1978**, *12*, 459. (c) Smith, D. F.; McIver, C. D.; Kleindienst, T. E. *J. Atmos. Chem.* **1998**, *30*, 209. (d) Klotz, B.; Sorensen, S.; Barnes, I.; Becker, K. H.; Etzkorn, T.; Volkamer, R.; Platt, U.; Wirtz, K.; Martin-Reviejo, M. *J. Phys. Chem.* **1998**, *102*, 10289. (e) Atkinson, R.; Aschmann, S. M. *Int. J. Chem. Kinet.* **1994**, *16*, 929.
(14) Volkamer, R.; Platt, U.; Wirtz, K. *J. Phys. Chem.* **2001**, *105*, 7865.
(15) Andino, J. M.; Smith, J. N.; Flagan, R.; Goddard, W. A.; Seinfeld, J. H. *J. Phys. Chem.* **1996**, *100*, 10967.
(16) Bartolotti, L. J.; Edney, E. O. *Chem. Phys. Lett.* **1995**, *245*, 119.
(17) Uc, V. H.; Garcia-Cruz, I.; Hernandez-Laguna, A.; Vivier-Bunge, A. *J. Phys. Chem.* **2002**, *104*, 7847.
(18) Suh, I.; Zhang, D.; Zhang, R.; Molina, L. T.; Molina, M. J. *Chem. Phys. Lett.* **2002**, *364*, 454.
(19) Frisch, M. J.; Trucks, G. W.; Schlegel, H. B.; Scuseria, G. E.; Robb, M. A.; Cheeseman, J. R.; Zakrzewski, V. G.; Montgomery, J. A., Jr.; Stratmann, R. E.; Burant, J. C.; Dapprich, S.; Millam, J. M.; Daniels, A. D.; Kudin, K. N.; Strain, M. C.; Farkas, O.; Tomasi, J.; Barone, V.; Cossi, M.; Cammi, R.; Mennucci, B.; Pomelli, C.; Adamo, C.; Clifford, S.; Ochterski, J.; Petersson, G. A.; Ayala, P. Y.; Cui, Q.; Morokuma, K.; Malick, D. K.; Rabuck, A. D.; Raghavachari, K.; Foresman, J. B.; Cioslowski, J.; Ortiz, J. V.; Stefanov, B. B.; Liu, G.; Liashenko, A.; Piskorz, P.; Komaromi, I.; Gomperts, R.; Martin, R. L.; Fox, D. J.; Keith, T.; Al-Laham, M. A.; Peng, C. Y.; Nanayakkara, A.; Gonzalez, C.; Challacombe, M.; Gill, P. M. W.; Johnson, B. G.; Chen, W.; Wong, M. W.; Andres, J. L.; Head-Gordon, M.; Replogle, E. S.; Pople, J. A. *Gaussian 98*, revision D.3; Gaussian, Inc.: Pittsburgh, PA, 1998.

reactions relevant to organic radical compounds.[20] The procedure involved determination of a correction factor associated with basis set effects at the MP2 level and subsequent correction to the energy calculated at a higher level of electron correlation with a moderate size basis set. A correction factor, CF, was determined from the energy difference between the MP2/6-31G(d) and MP2/6-311++G(d,p) levels. The values of calculated energies at the CCSD(T)/6-31G(d) level were then corrected by the MP2 level correction factors, corresponding to the CCSD(T)/6-31G(d) + CF level of theory.[20] The geometries of the OH−toluene adducts and their corresponding transition states were also fully optimized at the CASSCF level of theory to compare the calculated B3LYP and CASSCF geometries. The wave function was constructed for configurations made by all possible occupancies of the active electrons in the subspace of all active orbitals. In addition, for a few limited cases, we considered the MPW1K functional described previously by Truhlar and co-workers.[21] This approach was evaluated for a series of H-abstraction reactions.

Our recent work has evaluated the quantum chemical methods applicable to the aromatic intermediate radicals.[18] For the initial OH addition to toluene, we obtained the equilibrium structures and energetics of the OH−toluene adduct isomers and their corresponding transition states by using density function theory (B3LYP/6-31G(d,p)) and ab initio multiconfigurational calculations (CASSCF) for geometry optimization and second-order MP2 and coupled-cluster theory (CCSD(T)) for single-point energy calculations.[18] The results revealed that the DFT method predicted binding energies and activation energies in good agreement with the experimental values. The calculated rate constants and isomeric branching ratios for the formation of OH−toluene adducts using B3LYP/6-31G(d,p) structures and energetics were consistent with the experimental rate constant of the OH−toluene reaction and the measured cresol yields. On the other hand, the correlated methods employing MP2 and CCSD(T) produced significantly higher activation energies than the experimental value. The failure using the MP2 and CCSD(T) methods was explained by significant contamination of unrestricted Hartree−Fock wave function from higher spin states in the single-point energy calculations of the transition states. The performance of CASSCF and CSSPT2 was also unsatisfactory, producing higher activation energies than the experimental value.

Rate constants of unimolecular (k_{uni}) and bimolecular (k_b) reactions of the aromatic intermediate radicals were calculated using classic TST. The high-pressure limit unimolecular rate constant is expressed by:[22]

$$k_{uni} = \frac{kT}{h}\frac{Q^{\ddagger}_{AB}}{Q_{AB}}\exp\left(-\frac{E_a}{kT}\right) \quad (1)$$

where $Q^{\ddagger}_{AB}$ is the partition function of the transition state with the vibrational frequency corresponding to the reaction coordinate removed, Q_{AB} is the partition function of the reactant, and E_a is the zero-point corrected activation energy. The association rate is related to the dissociation rate by the equilibrium constant (K):[22]

$$\frac{k_{rec}}{k_{uni}} = K = \frac{Q_{AB}}{Q_A Q_B}\exp\left(\frac{D_0}{kT}\right) \quad (2)$$

where Q_{AB} is the partition function of the dissociating species, Q_A and Q_B are the partition functions of the fragmentation products, and D_0 is the zero-point corrected binding energy.

To assess the fate of chemically excited aromatic radicals, we evaluated their stabilization and unimolecular isomerization using RRKM/master equation. Briefly, the concentration of a species formed by chemical activation is related to the balance over all gain and loss processes:[23]

$$\frac{dn_i}{dt} = Rf_i - \omega n_i + \omega\sum_j P_{ij}n_j - \sum_r k_{ri}n_i \quad (3)$$

where n_i is the concentration of the intermediate having internal energy E_i, R is the overall formation rate, f_i is the normalized energy distribution, P_{ij} is the energy-transfer probability from j to i, k_{ri} is the reaction rate constant for the pathway r, and ω is the collision frequency.[23] Exact state counts for vibration density of states were evaluated by using the Beyer−Swinehart algorithm.[24] The RRKM/ME calculations employed an exponential model for collision energy transfer using an average energy grain of 250 cm^{-1}.[23] All vibrations were treated as harmonic. We found that explicit treatment of the internal rotors as hindered rotors did not significantly alter the results. Calculations were performed at fixed total angular momentum and subsequently Boltzmann averaged. The master equation calculations were performed for the primary peroxy radicals and bicyclic radicals.

Results and Discussion

Primary Peroxy Radicals. O_2 addition to the ortho OH−toluene adduct forms three possible structural isomers of the peroxy radicals (Scheme 1). Also, O_2 addition to the para OH−toluene adduct results in two plausible peroxy radical isomers. Figure 1 depicts the optimized geometries of the lowest-energy conformations of the peroxy radicals obtained using B3LYP/6-31G(d,p). The evaluation of the vibrational frequencies confirmed that all geometries reported represent minima on the potential energy surfaces.

For the peroxy radicals, the energetically favorable conformation corresponds to O_2 addition on the same side of the benzene ring as the hydroxyl group. Figure 1 shows that there exists intramolecular hydrogen binding in the peroxy radicals. It involves interaction between the terminal oxygen of the peroxy group and the hydrogen of the OH group, forming a six-membered ring. The distance of intermolecular hydrogen binding ranges from 1.90 to 1.95 Å.

Zero-point corrected reaction energies for the formation of the peroxy radicals are listed in Table 1, obtained at the B3LPY/6-31G(d,p) level of theory. Addition of O_2 to OH−toluene adducts leads to formation of the peroxy radicals with comparable relative stability within 2 kcal mol^{-1}. The binding energies of the peroxy radicals range from 3 to 6 kcal mol^{-1}. For the ortho OH−toluene adduct, O_2 addition at C3 of the aromatic ring represents the most stable isomer (PO3). It is clear that hydrogen binding plays a role in stabilizing the peroxy radicals: the hydrogen bond lengths are 1.93, 1.90, and 2.33 Å for PO1, PO3, and PO5, respectively, correlating with their relative stability. To survey basis set and electronic correlation effects on the binding energies of the peroxy radicals, we performed additional calculations for PO3 using several other methods, including MP2 and CCSD(T) for single-point energies and CASSCF and MPW1K for geometry optimization and energy calculations. The results are provided in Table 2. The

(20) (a) Lei, W.; Derecskei-Kovacs, A.; Zhang, R. *J. Chem. Phys.* **2000**, *113*, 5354. (b) Lei, W.; Zhang, R. *J. Chem. Phys.* **2000**, *113*, 153. (c) Suh, I.; Lei, W.; Zhang, R. *J. Phys. Chem.* **2001**, *105*, 6471. (d) Zhang, D.; Zhang, R. *J. Am. Chem. Soc*. **2002**, *124*, 2692.
(21) Lynch, B. J.; Fast, P. L.; Harris, M.; Truhlar, D. G. *J. Phys. Chem*. **2000**, *104*, 4811.
(22) (a) Lei, W.; Zhang, R. *J. Phys. Chem*. **2001**, *105*, 3808. (b) Zhang, D.; Zhang, R.; Allen, D. T. *J. Chem. Phys*. **2003**, *118*, 1794. (c) Zhang, D.; Zhang, R. *J. Chem. Phys*. **2002**, *116*, 9721.
(23) (a) Zhang, D.; Lei, W.; Zhang, R. *Chem. Phys. Lett*. **2002**, *358*, 171. (b) Lei, W.; Zhang, D.; Zhang, R.; Molina, L. T.; Molina, M. J. *Chem. Phys. Lett.* **2002**, *357*, 45. (c) Zhao, J.; Zhang, R.; North, S. W. *Chem. Phys. Lett.* **2003**, *369*, 204.
(24) Stein, S. E.; Rabinovitch, B. S. *J. Chem. Phys*. **1973**, *58*, 2438.

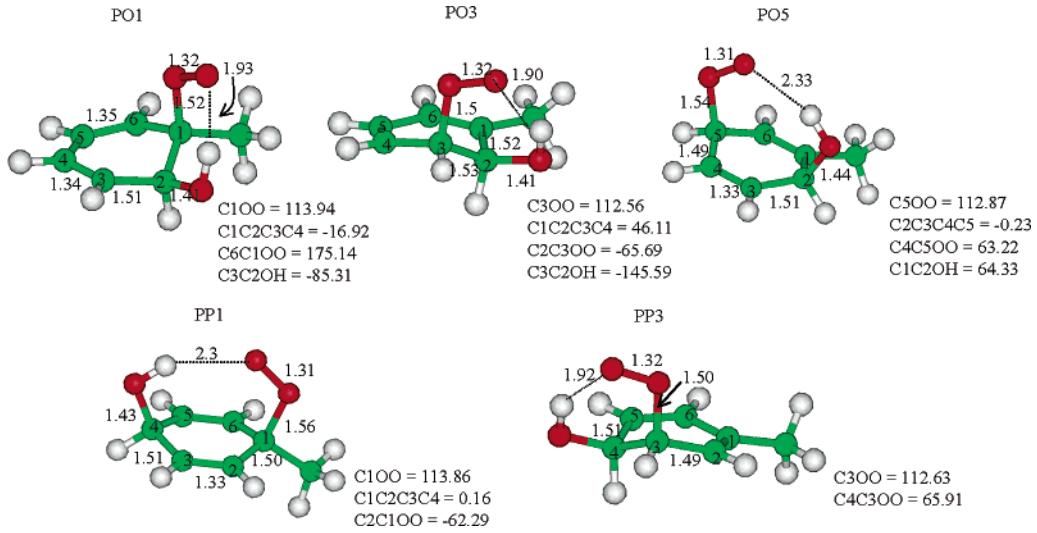

Figure 1. Structures of primary peroxy radicals at the B3LYP/6-31G(d,p) level of theory.

Table 1. Zero-Point Corrected Reaction Energies (RE in kcal mol^{-1}) and Activation Energies (E_a in kcal mol^{-1}) for the OH−Toluene−O_2 Reaction System[a]

type	reaction	RE	E_a	type	reaction	RE	E_a
ortho	PO1	−4.3	3.5	para	PP1	−4.0	−0.4
	PO3	−5.7	4.6		PP3	−5.8	4.6
	PO5	−3.9	0.3		PP1 → BP13	11.3	28.9
	PO5 → BO15	12.2	29.2		PP3 → BP35	−6.4	10.7
	PO1 → BO14	14.5	23.4		PP3 → BP36	14.8	23.7
	PO1 → BO13 (a)	−8.0	9.0		BP13 → EP1_23	−32.9	
	PO3 → BO13 (b)	−6.6	10.4		BP35 → EP3_56	−16.2	16.5
	PO3 → BO36	15.6	24.4		BP35 + O_2 → P_BP35_2	−14.7	1.4
	PO5 → BO35	12.1	31.4	ipso	PI2	−3.1	6.0
	BO14 → EO1_34	−36.7			PI4	−3.4	1.0
	BO13 → EO3_16	−16.6	16.4		PI2 → BI24	10.7	30.3
	BO35 → EO5_34	−33.8			PI2 → BI25	13.2	22.1
	BO35 → EO3_45	−31.0			PI2 → BI26	−9.0	9.5
	BO15 → EO5_16	−35.7			PI4 → BI46	11.6	29.6
	BO15 → EO1_56	−29.9			BI24 → EI2_34	−16.3	
	BO13 + O_2 → P_BO13_4	−13.7	2.0		BI25 → EI2_45	−38.5	
	BO13 + O_2 → P_BO13_6	−12.9	2.1		BI26 → EI2_56	−11.2	15.0
meta	PM2	−5.6	5.0		BI45 → EI4_56	−34.6	
	PM4	−5.7	5.2				
	PM6	−6.1					

[a] All calculations were based on B3LYP/6-31G(d,p) optimized geometries. Zero-point energy (ZPE) corrections were calculated at the B3LYP/6-31G(d,p)//B3LYP/6-31G(d,p) level of theory.

Table 2. Binding Energies (D_o), Activation Energies (E_a), Rate Constants (k), Equilibrium Constants (k_{eq}), and Spin Eigenvalues ($\langle S^2 \rangle$) for Peroxy Radical PO3 Calculated by Using Various Quantum Chemical Methods

method	D_o (kcal mol^{-1})	$\langle S^2 \rangle^a$	E_a (kcal mol^{-1})	$\langle S^2 \rangle^b$	k (cm^3 molecule^{-1} s^{-1})	K_{eq} (cm^3 molecule^{-1})
B3LYP/6-31G(d,p)	5.7	0.75 (0.75)	4.6	0.98 (0.76)	1.1×10^{-17}	1.8×10^{-23}
CCSD(T)/6-31G(d)	10.0	0.76 (0.75)	11.3	2.14 (2.54)	1.7×10^{-22}	2.4×10^{-20}
CCSD(T)/6-31G(d) + CF	8.9		12.9		1.6×10^{-23}	3.8×10^{-21}
MPW1K[c]	4.9	0.76 (0.75)	11.7	1.30 (0.84)	6.8×10^{-23}	4.7×10^{-24}
CASSCF	1.8		9.5		2.7×10^{-21}	2.2×10^{-26}

[a] Spin eigenvalues before (after) spin projection for the formation of PO3. [b] Spin eigenvalues before (after) spin projection for the transition state of PO3. [c] Frequency calculations were based on MPWPW91/6-31G(d,p)//MPWPW91/6-31G(d,p).

binding energies predicted by MPW1K and CASSCF are lower than that of B3LYP/6-31G(d,p) by 0.8 and 3.9 kcal mol^{-1}, respectively. On the other hand, the CCSD(T)/6-31G(d) method predicts a binding energy by 4.3 kcal mol^{-1} larger than the B3LYP/6-31G(d,p) value. Inclusion of the basis set correction method for CCSD(T)/6-31G(d) slightly reduces the binding energy. Spin contamination in the calculations of the peroxy radicals using the various quantum chemical methods is insignificant. The spin eigenvalues, $\langle S^2 \rangle$, are 0.760 for CCSD(T)/6-31G(d), 0.755 for MPW1K, and 0.75 for B3LYP/6-31G(d,p) before spin projection, nearly identical to the exact value of a pure doublet. Additional calculations of the binding energies of the peroxy radicals using CCSD(T)/6-31G(d) are presented in Table 3. In all cases, the binding energies of the peroxy radicals predicted by using CCSD(T)/6-31G(d) are higher than those obtained with B3LYP/6-31G(d,p).

Several previous theoretical studies have investigated OH−O_2−toluene peroxy radicals. Using a method involving semiempirical UHF/PM3 geometry optimization followed by B3LYP/

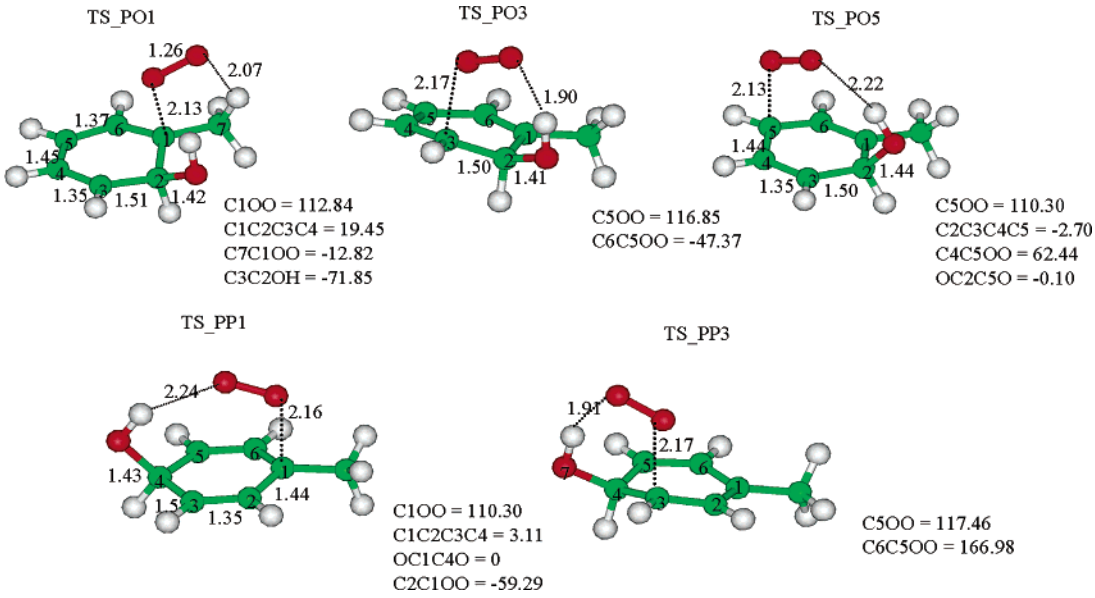

Figure 2. TS structures of primary peroxy radicals at the B3LYP/6-31G(d,p) level of theory.

Table 3. Binding Energies (D_0) and Equilibrium Constants (k_{eq}) of Selected Peroxy Radicals Calculated by Using CCSD(T)/6-31G(d)

species	D_0 (kcal mol^{-1})	$\langle S^2 \rangle^a$	k_{eq} (cm^3 molecule^{-1})
PO3	10.0	0.76 (0.75)	2.4×10^{-20}
PP3	10.4	0.76 (0.75)	5.5×10^{-21}
PI2	8.1	0.76 (0.75)	1.3×10^{-21}
			$(3.25 \pm 0.33) \times 10^{-19}$[b]

[a] Spin eigenvalues before (after) spin projection. [b] Experimental value from ref 12.

6-31G(d,p) single-point energy calculations, Andino et al. considered the peroxy radicals with O_2 being added to the opposite side of the toluene ring relative to the OH group and obtained the binding energies of 3−5 kcal mol^{-1}.[15] A recent study by Garcia-Cruz et al. investigated the configurations with O_2 being added to both the same and opposite sides of the ring relative to the OH group using B3LYP/6-31G(d) and PMP2.[9] The authors concluded that the configuration with OH and O_2 on the same side of the ring results in a stabilization of 1.5−3.0 kcal mol^{-1} for the peroxy radicals. Our structures and binding energies of the peroxy radicals obtained by using B3LYP/6-31G(d,p) are consistent with those reported by Garcia-Cruz et al. using B3LYP/6-31G(d). Another theoretical study by Bartolotti and Edney calculated much larger binding energies for O_2 addition to the ortho OH−toluene adduct using density functional theory, ranging from 18 to 23 kcal mol^{-1}.[16] For comparison, the binding energy of the analogous OH−benzene peroxy radical was predicted to be 8.2 and 5.2 kcal mol^{-1} using B3LYP/6-31(+)G(d) and B3LYP/6-311+G(d)//B3LYP/6-31(+)G(d), respectively.[25] Using a combined thermochemical group additivity rules and semiempirical UHF/PM3 method, Lay et al. obtained a slightly larger binding energy of 12 kcal mol^{-1} for the OH−benzene peroxy radical.[26]

The transition state (TS) leading to the formation of the peroxy radical was searched by using the TS keyword in geometry optimization at the B3LYP/6-31G(d,p) level of theory. The C−O bond length was successively increased relative to the equilibrium structures of the corresponding peroxy radical. Once an initial geometry optimization reached convergence, a frequency calculation was performed to determine whether this optimized geometry represented a first-order saddle point. A transition state was identified by finding only one imaginary component in the calculated vibrational frequencies. The vibrational modes along the reaction coordinates were examined to verify that these modes represented the trend along the intended reaction coordinate. At the B3LYP/6-31G(d,p) level of theory, we performed additional calculations using the intrinsic reaction coordinate (IRC) method, confirming that each TS uniquely connected the reactant to the product. The TS structures for the formation of peroxy radicals are illustrated in Figure 2. The C−O bond lengths at the transition states range from 2.13 to 2.17 Å. Intramolecular hydrogen binding also exists in the TS structures. The hydrogen bond lengths are between 1.88 and 2.24 Å, with the latter value corresponding to rather weak hydrogen binding. Note that the hydrogen bond in TS_PO1 goes to the neighboring methyl group, which is due to the interaction of the lone pairs between the oxygen atom in the peroxy group and the hydrogen atom in the methyl group. The oxygen bond rotates to shorten the distance between O and H in the methyl group. On the other hand, the distance between the O atom in the peroxy group and the H atom in hydroxyl group is 2.51 Å.

The activation energies to form the peroxy radicals are also included in Table 1. The activation barriers of O_2 addition to the ortho OH−toluene adduct are less than 5 kcal mol^{-1}. It is interesting to note that, although the peroxy radical PO3 represents the most stable form for ortho OH addition, its activation energy is slightly higher than those of PO1 and PO5. We also examined basis set and electronic correlation effects on the barrier heights for PO3 (Table 2). The CCSD(T)/6-31G(d) and CCSD(T)/6-31G(d) + CF methods both predict higher activation energies than the B3LYP/6-31G(d,p) method, by 6.7 and 8.3 kcal mol^{-1}, respectively. The MPW1K and CASSCF barrier heights are also higher than the B3LYP value, but are slightly less than the CCSD(T) values. Spin contamination in calculating the TS energy using CCSD(T) is significant, with the $\langle S^2 \rangle$ value of 2.13 before the $S + 1$ component being

(25) Ghigo, G.; Tonachini, G. *J. Am. Chem. Soc.* **1998**, *120*, 6753.
(26) Lay, T. H.; Bozzelli, J. W.; Seinfeld, J. H. *J. Phys. Chem.* **1996**, *100*, 6543.

Table 4. Calculated High-Pressure Limit Rate Constants of Stabilized Aromatic Radicals for the OH−Toluene−O_2 Reaction System at 300 K[a]

species	k_b	A-factor	k_{uni}	A-factor	species	k_b	A-factor	k_{uni}	A-factor
PO1	5.2×10^{-17}	2.0×10^{-14}	1.9×10^{8}	9.1×10^{13}	PP1	3.7×10^{-15}	1.9×10^{-15}	3.8×10^{10}	1.6×10^{13}
PO3	1.2×10^{-17}	2.6×10^{-14}	6.3×10^{5}	2.0×10^{13}	PP3	1.4×10^{-18}	3.4×10^{-15}	5.1×10^{5}	2.2×10^{13}
PO5	1.2×10^{-14}	1.8×10^{-14}	1.0×10^{10}	1.2×10^{13}	BP35			2.0×10^{4}	1.3×10^{12}
BO13 (a)			1.9×10^{6}	6.8×10^{12}	EP3_56			4.5	4.8×10^{12}
BO13 (b)			2.9×10^{4}	1.1×10^{12}	P_BP35_2	8.5×10^{-15}	9.5×10^{-14}		
EO3_16			6.8	5.7×10^{12}	P12	8.1×10^{-19}	2.0×10^{-14}	2.6×10^{6}	1.2×10^{13}
P_BO13_4	4.4×10^{-15}				BI26			9.2×10^{4}	7.8×10^{11}
P_BO13_6	1.9×10^{-15}				EI2_56			1.8×10^{2}	9.3×10^{12}

[a] Using B3LYP/6-31G(d,p) results. Unimolecular rate constants are in s^{-1}, and bimolecular rate constants are in cm^3 $molecule^{-1}$ s^{-1}. The A-factor is in s^{-1} for unimolecular reactions and cm^3 $molecule^{-1}$ s^{-1} for bimolecular reactions.

annihilated, rendering this method unreliable. The MPW1K method also suffers from spin contamination, with a $\langle S^2 \rangle$ value of 1.26 before annihilation. For the B3LYP/6-31G(d,p) method, the $\langle S^2 \rangle$ values are 0.98 and 0.76 before and after annihilation, respectively. It should be pointed out that calculations of geometries and energetics of the transition states of the peroxy radicals using CASSCF and CCSD(T) are computationally extremely consuming, and it is unrealistic to employ both methods for each species investigated in this work. The study by Andino et al. reported the activation barriers of 8−10 kcal mol^{-1} for the OH−toluene peroxy radicals, somewhat higher than our B3LYP/6-31G(d,p) values.

We calculated the high-pressure limit rate constants of O_2 addition to the OH−toluene adducts, using the classic TST and the structures and energetics obtained with B3LYP/6-31G(d,p). As presented in Table 4, the calculated rate constants range from 10^{-14} to 10^{-18} cm^3 $molecule^{-1}$ s^{-1}, showing distinct kinetics for the isomers of the peroxy radicals. For the ortho OH adduct, O_2 addition occurs with the rate constants of 5.2×10^{-17}, 1.2×10^{-17}, and 1.0×10^{-14} cm^3 $molecule^{-1}$ s^{-1} for PO1, PO3, and PO5, respectively. Several experimental studies have reported the O_2 addition rate constant to the OH−toluene adduct.[10a,12] Early studies indirectly inferred this rate by fitting OH decay in the presence of toluene and O_2 and assuming a triexponential formulation and determined the rate constant of $(5-6) \times 10^{-16}$ cm^3 $molecule^{-1}$ s^{-1} at room temperature.[10a] A more recent work by Bohn investigated the kinetics of the OH−toluene adduct with O_2 by monitoring the OH−toluene adduct using cw UV-laser long path absorption and reported a larger rate constant of $(3 \pm 2) \times 10^{-15}$ cm^3 $molecule^{-1}$ s^{-1}.[12] Our calculated rate constants of the reactions of the OH−toluene adducts with O_2 encompass the previous experimental values but suggest strong isomeric and multiexponential kinetic effects which are unaccounted for in the previous experimental studies. It is also clear from Table 2 that the activation barriers predicted by CCSD(T), MPW1K, and CASSCF are significantly higher, yielding much lower rate constants than the experimental values. Apparently, the CCSD(T) method produces erroneous activation barriers because of significant spin contamination.

Equilibrium between formation and decomposition of the peroxy radicals was evaluated according to eq 2. Using the B3LYP/6-31G(d,p) results, we calculated the equilibrium constants to range from 10^{-23} to 10^{-24} cm^3 $molecule^{-1}$ for the peroxy radicals with ortho and para OH additions. The equilibrium constants of the peroxy radicals predicted by the various methods are contained in Tables 2 and 3. The recent experimental work by Bohn reported an equilibrium constant of $(3.25 \pm 0.33) \times 10^{-19}$ cm^3 $molecule^{-1}$ for OH−O_2−toluene peroxy radicals (Table 3).[12] The experimental equilibrium was derived by fitting the measured OH−toluene adduct signal with a multiexponential expression assuming a single OH−toluene adduct, hence not differentiating the isomeric effect. The experimental equilibrium constant is significantly higher than our B3LYP/6-31G(d,p) values, but is closer to our CCSD(T) values. It is plausible that the binding energies predicted by the CCSD(T) method are more reliable than the B3LYP method, considering the fact that spin contamination is not significant in the energy calculations of the peroxy radicals associated with the CCSD(T) method (Tables 2 and 3). The calculated equilibrium constant for PO3 obtained with CCSD(T) is about a factor of 10 higher than the experimental value reported by Bohn. As reflected by eq 2, the equilibrium constant is strongly dependent on binding energies of the peroxy radicals. The accuracy in the predicted energetics of the quantum chemical calculations is estimated to be within 1−2 kcal mol^{-1}.[20] Hence, the binding energies predicted by the CCSD(T) method appear to be consistent with the experimental value, considering the respective uncertainties.

Because of the relatively small binding energies of the peroxy radicals, the OH−toluene adduct reaction with O_2 proceeds reversibly, and the equilibrium favors peroxy radical decomposition. The close relative stability and reversibility of the peroxy radicals suggest that all isomers of the peroxy radicals are likely to form. The relative stability and activation barriers of the peroxy radicals, however, have little effect on isomeric branching, since propagation of the toluene oxidation is largely determined by the exit channel of the peroxy radicals. The steady-state concentrations of the peroxy radicals are determined by recombination of the adduct with O_2, dissociation of the peroxy radicals, and the exit channel of the peroxy radicals, that is, reaction with NO to form alkoxy radicals or rearrangement to form bridged bicyclic radicals.

Bicyclic Radicals. For ortho OH addition, peroxy radicals PO1 and PO3 each likely cyclize to form three possible bridged bicyclic radicals, and peroxy radical PO5 likely cyclizes to form two possible bicyclic radicals. Also, cyclization of PO1 and PO3 (PO3 and PO5) leads to an identical bicyclic radical BO13 (BO35). Formation of BO13 from PO1 and PO3 involves a five-membered oxygen ring, with initial O_2 attachment to a tertiary and secondary site and subsequent C−O closure to a secondary and tertiary site, respectively. Hence, there exist five plausible bicyclic radicals from ortho OH addition. Similarly, three possible bicyclic radicals are likely resulted from para OH addition.

Figure 3 shows the equilibrium structures and transition states of bicyclic radicals BO13 and BP35. The TS structures leading

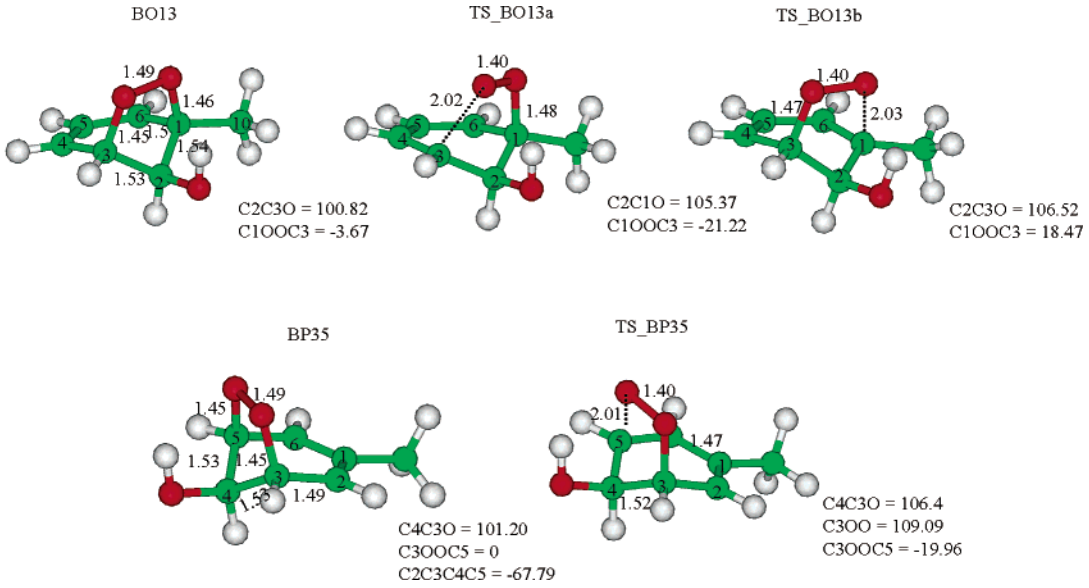

Figure 3. Structures of bicyclic radicals and their corresponding transition states at the B3LYP/6-31G(d,p) level of theory.

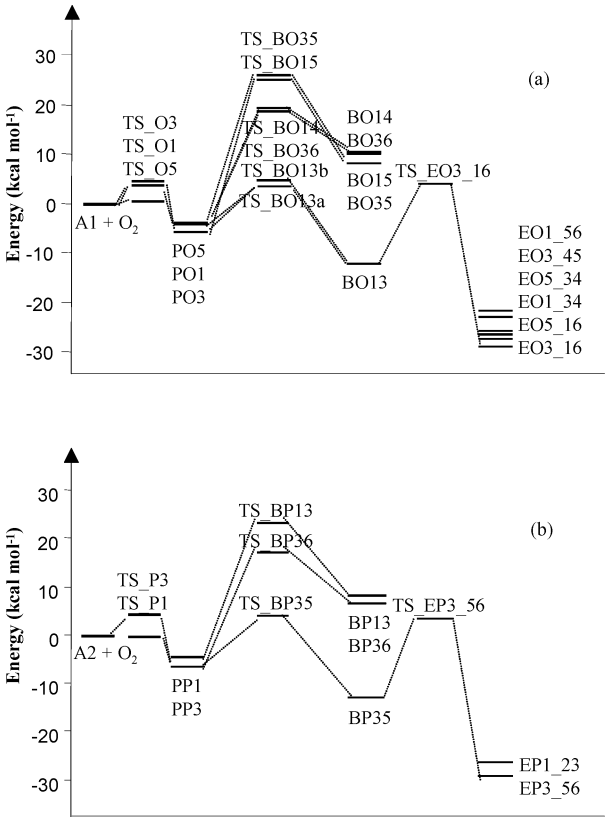

Figure 4. PES involving primary peroxy, bicyclic, and epoxy radicals for ortho (a) and para (b) OH addition obtained by using B3LYP/6-31G(d,p).

to BO13 formation from PO1 and PO3 are similar, with the exception of the bridged C−O bond distances and the dihedral angle C1OOC3. The distances for C−O closure at the transition states are 2.02 and 2.03 Å for PO1 and PO3, respectively. The reaction and activation energies for isomerization of peroxy to bicyclic radicals are presented in Table 1. The potential energy surface (PES) of the peroxy to bicyclic radical isomerization is illustrated in Figure 4.

The results from Table 1 and Figure 4 indicate that, unlike the primary peroxy radicals, the bridged bicyclic radicals exhibit distinct stability patterns. For ortho OH addition, the bicyclic

Table 5. Calculations of Reaction Energies (RE), Activation Energies (E_a) for the Formation of Bicyclic BO13 and Epoxide EO3_16

	CASSCF		CCSD(T)/6-31G(d)		CCSD(T)/6-31G(d) + CF	
reaction	RE	E_a	RE	E_a	RE	E_a
PO3 → BO13	−27.2	12.2	−10.5	12.5	−9.7	13.1
BO13 → EO3_16	−24.6	19.6	−18.2	28.0	−19.1	27.3

radical formed by O_2 addition at C1 and subsequent bridge formation at C1 and C3 (BO13) is most stable, while the other bicyclic radicals possess structures that are about 20 kcal mol^{-1} higher in energy. Similarly, for para OH addition, the bicyclic radical BP35 represents the most stable form and is located about 20 kcal mol^{-1} below its other two structural isomers. The high stability of BO13 and BP35 is explained since both structures possess a delocalized allyl-π system, while their other structural isomers possess only one localized double bond.[9,15]

Formation of the nonallylically stabilized bicyclic radicals occurs via high-lying transition states, and the activation barriers are 10−20 kcal mol^{-1} higher than those of BO13 and BP35. At the B3LYP/6-31G(d,p) level of theory, isomerization of PO3 to BO13 is exothermic by about 7 kcal mol^{-1} and occurs with an activation barrier of about 10 kcal mol^{-1}. The exothermicity and activation barrier for BO13 from PO1 are both about 1.4 kcal mol^{-1} less than those from PO3. The reaction and activation energies of BP35 are very similar to those of BO13. The previous theoretical work by Andino et al. reported the activation energies of 17.2 and 12.4 kcal mol^{-1} for isomerization of PO3 and PO1 to BO13, respectively, by 6.9 and 3.4 kcal mol^{-1} higher than our B3LYP/6-31G(d,p) values.[15] Additional calculations using CASSCF, CCSD(T)/6-31G(d), and CCSD(T)/6-31G(d) + CF yielded slightly higher activation energies of PO3 to BO13 isomerization, but these results are within 2.7 kcal mol^{-1} of the B3LYP/6-31G(d,p) barrier height (Table 5). In addition, except for the CASSCF method which predicts a higher stability, the reaction energies predicted by the CCSD(T) methods are within 4 kcal mol^{-1} of the B3LYP/6-31G(d,p) value. Spin contamination associated with calculations of the bicyclic radicals and their corresponding TS's using the B3LYP/6-31G(d,p) method is minimal: for BO13 the $\langle S^2 \rangle$

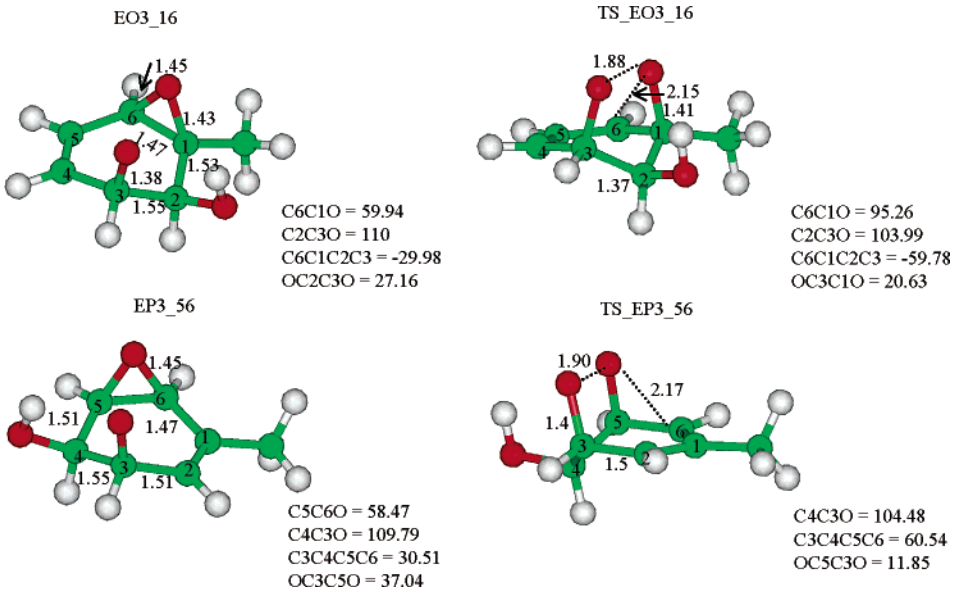

Figure 5. Structures of epoxy radicals and their corresponding transition states at the B3LYP/6-31G(d,p) level of theory.

values are 0.78 and 0.75 before and after spin projection, respectively. At the CCSD(T)/6-31G(d) level of theory, the $\langle S^2 \rangle$ values before (after) spin projection are 0.937 (0.759) for BO13 and 1.333 (0.958) for its corresponding TS.

Since the reaction of the OH−toluene adduct with O_2 is exoergic, the peroxy radicals produced are vibrationally excited. There are three possible reaction pathways for the excited peroxy radicals: collisional stabilization, prompt isomerization to the bicyclic radical, or prompt dissociation to the OH−toluene adduct. We performed calculations to assess the fate of the excited peroxy radicals using the RRKM/ME formalism. The master equation analysis predicted predominant stabilization for the peroxy radicals, with a negligible fraction of prompt unimolecular reactions. The dominance of stabilization for the peroxy radicals is not surprising, considering the nearly identical barrier heights between cyclization to the bicyclic radicals and decomposition to the OH−toluene adducts.

Using the B3LYP/6-31G(d,p) results, we calculated the unimolecular rate constants of the stabilized peroxy radicals (Table 4). The rate constants for isomerization of thermalized PO3 and PO1 to BO13 are 3×10^4 and 1.9×10^6 s^{-1}, respectively. Formation of bicyclic radical BP35 has a rate of 2.0×10^4 s^{-1}. In the atmosphere, there are two competing exit pathways for the primary peroxy radicals, i.e., isomerization to bicyclic radicals or reaction with NO to form alkoxy radicals and NO_2. We estimated a first-order rate of about 2 s^{-1} for the peroxy radical reaction with NO, assuming a rate constant on the order of 10^{-11} cm^3 $molecule^{-1}$ s^{-1} for the NO−peroxy radical reaction and an ambient NO mixing ratio of 10 ppb typical of a polluted urban atmosphere.[1−3] Isomerization of peroxy radical PO1 or PO3 to bicyclic radical BO13 is significantly faster than the competing reaction with NO. The dominance of the bicyclic radical formation over the alkoxy radical formation from the primary peroxy radicals remains unchanged, even if the CASSCF or CCSD(T) results are considered. The activation barriers for decomposition and isomerization of the peroxy radicals are comparable (Table 1). The decomposition rate of PO1 or PO3 to the OH−toluene adduct is larger than that of isomerization to the bicyclic radical because of larger A-factors associated with decomposition (Table 4). The experimental study by Bohn observed an irreversible loss of the OH−toluene adduct that could not be interpreted by simply considering the equilibrium between the adduct and peroxy radicals.[12] The author attributed this loss to two possible pathways, i.e., an additional irreversible reaction of the adduct with O_2 with a bimolecular rate constant of $(6.0 \pm 0.5) \times 10^{-16}$ cm^3 $molecule^{-1}$ s^{-1} and a unimolecular rate of $(1.85 \pm 0.15) \times 10^3$ s^{-1} for the peroxy radical. Our calculated unimolecular isomerization rates of PO3 and BP35 are 2.9×10^4 and 2.0×10^4 s^{-1}, respectively, using B3LYP/6-31G(d,p). Those rates for the exit channel of the peroxy radical (that is, the formation of the bicyclic radical) are apparently consistent with the experimentally proposed unimolecular rate for the exit channel of the peroxy radicals, considering the respective uncertainties in the theoretical and experimental studies.

Hence, despite the likely existence of all primary peroxy radical isomers, only the formation of the bicylic radical BO13 is allowed and is contributed by peroxy radicals PO1 and PO3. Isomerization of the peroxy radical to bicyclic radical BO13 represents the solely accessible isomeric pathway to propagate toluene oxidation for ortho OH addition. Similarly, for para OH addition, only the peroxy radical PP3 is able to cyclize to form the bicyclic radical BP35, and the peroxy radical cyclization dominates over the reaction with NO.

Epoxy Radicals. The high-lying transition states and unstable structures of the nonallylic bicyclic radicals render formation of the majority of the epoxy radicals atmospherically irrelevant (Schemes 1 and 2). For ortho OH addition, only the formation of epoxides EO1_34 and EO3_16 are plausible, both resulting from isomerization of BO13. For the para OH adduct, isomerization of bicyclic radical BP35 leads to epoxide EP3_56. The equilibrium structures of epoxides EO3_16 and EP3_56 are shown in Figure 5, along with their corresponding transition states. At the transition states, the distances for breaking the O−O bond are 1.88 Å for EO3_16 and 1.90 Å for EP3_56, and the distances for C−O closure are 2.15 Å for EO3_16 and 2.17 Å for EP3_56. The relative stability of the epoxy radicals

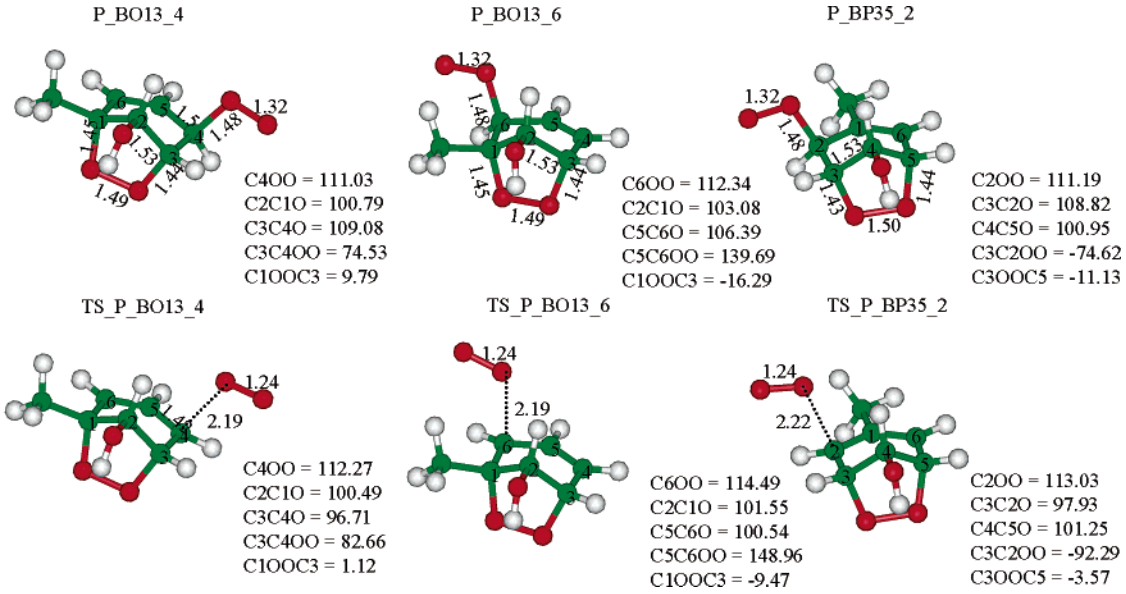

Figure 6. Structures of bicyclic peroxy radicals and their corresponding transition states at the B3LYP/6-31G(d,p) level of theory.

and the PES for bicyclic to epoxy radical isomerization are also shown in Figure 4.

The epoxy radicals are mostly noticeable for their high stability. The epoxides are about 16−37 kcal mol^{-1} more stable than their bicyclic precursors and about 16−23 kcal mol^{-1} more stable than their peroxy radical precursors (Table 1). For ortho OH addition, the epoxide EO3_16 is most stable, and the relative stability of the epoxides is within 7 kcal mol^{-1}. Epoxide EP3_56 is most stable for para OH addition. The activation barrier to form EO3_16 from BO13 is predicted to be 16.4 kcal mol^{-1}. We were unable to locate the transition state for formation of EO1_34 from BO13, but it is expected that the activation barrier for this epoxide is higher than that for EO3_16. Epoxide EO1_34 is about 3 kcal mol^{-1} less stable than EO3_16. Isomerization of BP35 to EP3_56 has a comparable barrier of 16.5 kcal mol^{-1}. The activation barriers for EP3_16 calculated with the CASSCF and CCSD(T) methods were higher than that with B3LYP/6-31G(d,p) (Table 5). The activation barrier is about 3 kcal mol^{-1} higher with CASSCF and 10−11 kcal mol^{-1} with CCSD(T). Spin contamination associated with the B3LYP/6-31G(d,p) method is unimportant for the epoxy radicals, with the $\langle S^2 \rangle$ value very close to 0.75 before projection. The $\langle S^2 \rangle$ value with CCSD(T)/6-31G(d) for EO3_16 is 0.86 (0.75) before (after) projection. However, spin contamination is of concern in the TS calculation of EO3_16 using CCSD(T), with the $\langle S^2 \rangle$ values of 1.90 and 1.46 before and after projection, respectively.

Because of the higher activation barriers, the calculated high-pressure limit rate constants for isomerization of the thermalized bicyclic radical to epoxide are small, ranging from 4 to 7 s^{-1} (Table 4) using the B3LYP/6-31G(d,p) energetics. Those rate constants are even smaller if the activation barriers predicted by CASSCF and CCSD(T) are considered (Table 5). The RRKM/ME formalism was employed to assess the fate of chemically excited bicyclic radicals. The calculations suggested dominant stabilization for the bicyclic radicals, with a negligible fraction of prompt unimolecular reactions to the primary peroxy radicals or epoxy radicals.

Bicyclic Peroxy Radicals. For ortho OH addition, we considered two bicyclic peroxy radicals, with O_2 addition at C4 and C6 to BO13, denoted as P_BO13_4 and P_BO13_6, respectively. For para OH addition, the bicyclic peroxy radical, P_BP35_2, with O_2 addition to C2 of BP35 was investigated. Geometry optimization and energy calculations of the bicyclic peroxy radicals were performed using the B3LYP/6-31G(d,p) method. The equilibrium structures for the bicyclic peroxy radicals and their corresponding transition states are shown in Figure 6. The PES for the bicyclic peroxy radicals is showed in Figure 7. The bicyclic peroxy radicals P_BO13_4 and P_BO13_6 are 12.9 and 13.7 kcal mol^{-1} more stable than BO13, and their activation barriers are 2.1 and 2.0 kcal mol^{-1}, respectively. The reaction and activation energies of P_BP35_2 are comparable, with the values of 14.7 and 1.4 kcal mol^{-1}, respectively. The binding energies of the bicyclic peroxy radicals are substantially larger than those of the corresponding primary peroxy radicals at the B3LYP/6-31G(d,p) level of theory. Spin contamination for the bicyclic peroxy radicals are minimal using B3LYP/6-31G(d,p). Spin contamination in the TS calculations of the bicyclic peroxy radicals is not negligible but is effectively removed after spin projection.

The calculated bimolecular rate constants for the formation of the bicyclic peroxy radicals range from 2×10^{-15} to 9×10^{-15} cm^3 molecule^{-1} s^{-1} (Table 4). O_2 addition to the bicyclic radical BO13 to form P_BO13_4 occurs about two times faster than that to form P_BO13_6.

Fate of Bicyclic Radicals: Isomerization vs O_2 Reaction. We now discuss the fate of the bicyclic radicals, i.e., the competition between isomerization to epoxides and O_2 addition to form bicyclic peroxy radicals. For both ortho and para addition pathways, isomerization of bicyclic radicals yields epoxide radicals which are slightly more stable than the bicyclic peroxy radicals (Figure 7). However, the activation barriers leading to the epoxides are significantly higher. The effective first-order rate constants of the reactions of bicyclic radicals with O_2 are about $(1-5) \times 10^4$ s^{-1}. Consequently, the O_2

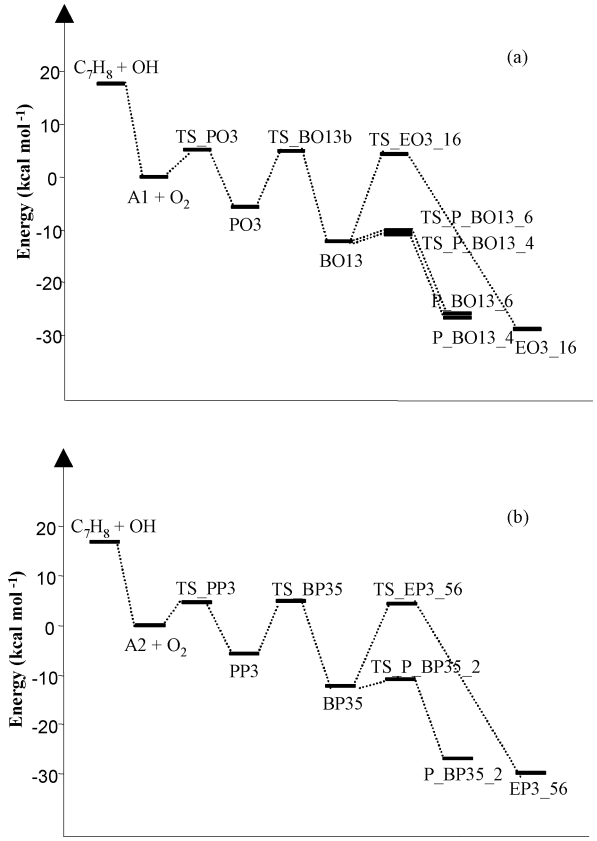

Figure 7. Overall PES of the OH−toluene reaction system for ortho (a) and para (b) OH addition obtained by using B3LYP/6-31G(d,p). As has been shown theoretically[17,18] and experimentally,[10] the OH−toluene reaction proceeds via a preactivation complex with negative activation energies. This is in contrast to the OH−benzene reaction which occurs with a small positive barrier.[27] The negative activation energy for the OH−toluene formation is not shown.

addition rate to form the bicyclic peroxy radical is nearly 4 orders of magnitude faster than that of epoxide formation, indicating that bicyclic radicals react exclusively by bimolecular reaction with O_2. The bicyclic peroxy radicals are then expected to react with NO to form the bicyclic alkoxy radicals and NO_2, which is important for ozone formation. The bicyclic alkoxy radicals subsequently undergo ring cleavage, leading to formation of glyoxal, methyl glyoxal, and several unsaturated anhydrides such as dihydro-2,5,-furandione, 2,5-furandione, and 3-methyl-2,5-furandione which have been detected as the primary SOA components.[3−5] The theoretical work by Lay et al. also assessed the formation of bicyclic radicals and bicylic peroxy radicals from OH−benzene reactions using the semiempirical UHF/PM3 method.[26]

The formation of epoxides was initially suggested because of their high stability.[16] On the basis of an environmental chamber study of the OH-initiated reactions of several alkylbenzenes using GC/MS detection, Jeffries and co-workers detected several mass peaks matching those of epoxide carbonyls.[6] The yields of those products, however, were observed to be small. Also, the authors suggested that positive identification of the epoxy carbonyls under actual experimental conditions required authentic standards. Hence, experimental evidence for the formation of epoxide radicals was rather inconclusive. A more recent theoretical work also suggested the nonplausibility of epoxide formation from oxidative degradation of benzene.[28]

Recently, Volkamer et al. investigated primary versus secondary glyoxal yields.[14] Their measurement of time-resolved glyoxal yield allowed for differentiation of primary and secondary glyoxal formation. Although glyoxal can be, in principle, produced from degradation of many intermediates including alkoxy, bicyclic peroxy, and epoxide radicals, only the pathway via the bicyclic peroxy radical leads to the primary formation on a relatively short time scale. The experimental study showed dominant primary glyoxal formation, with a yield of (39.0 ± 10.2)%. Hence, the experimental evidence suggests that the ortho addition pathway proceeds primarily via the bicyclic peroxy radical channel, in agreement with our theoretical prediction.

Our recent theoretical work[18] predicted the branching ratios of 0.52, 0.34, 0.11, and 0.03 for OH addition to ortho, para, meta, and ipso positions, respectively, indicating a strong preference of OH addition to the ortho and para positions. Using those branching ratios along with the kinetic results from this work predicted with the B3LYP/6-31G(d,p) level of theory, we estimated the yield for glyoxal formation. Our estimate of the glyoxal yield required information on cresol formation, which was based on previous experimental studies, with a total yield of about 18%.[13] Cresol formation occurs either by H-abstraction by O_2 from the OH−toluene adduct or by HO_2 elimination from the peroxy radicals. We predicted an upper limit of about 50% for the glyoxal yield, consistent with the experimental observation by Volkamer et al.[14]

Conclusions

The present theoretical results provide several new insights into the mechanism of toluene oxidation in the atmosphere. The thermochemical and kinetic data allow for a quantitative assessment of the formation potential of ozone, epoxide carbonyls, and SOA. The results explain previous product observations and provide guidance for future experimental and field studies to identify intermediates, stable products, and SOA components from the oxidation of toluene in the atmosphere.

(1) Our work confirms previous experimental and theoretical studies on the reversibility of the reaction OH−toluene adduct with O_2. The theoretical results suggest distinct isomeric effects for the rate constants and equilibrium constants of this reaction. The relative stability and activation barriers of the peroxy radicals, however, have negligible effect on the overall branching of the OH−toluene reactions, which is largely dependent on the exit channel of the primary peroxy radicals.

(2) The peroxy radicals mainly cyclize to produce the bicyclic radicals rather than react with NO, even in polluted air. Ozone production from the primary peroxy radicals is unimportant.

(3) At each OH attachment site, only one isomeric pathway via the bicyclic peroxy radical is accessible to lead to ring cleavage.

(4) Rearrangement of bicyclic radicals to more stable epoxides is too slow to matter because of the high activation barriers, and we conclude that there is negligible formation of epoxide carbonyls from the epoxide intermediates. Under atmospheric conditions, the bicyclic radicals react with O_2 to form the

(27) Lin, M. C.; Tokmakov, I. V. *J. Phys. Chem.* **2002**, *106*, 11309.
(28) Motta, F.; Ghigo, G.; Tonachini, G. *J. Phys. Chem.* **2002**, *106*, 4411.

bicyclic peroxy radicals (secondary). Subsequent reactions of the bicyclic peroxy radicals with NO produce NO_2 (hence, ozone) and bicyclic alkoxy radicals which then undergo ring cleavage to yield SOA precursors.

Acknowledgment. This work was partially supported by the Robert A. Welch Foundation (A-1417), Texas Air Research Center (TARC), and the DOE Atmospheric Chemistry Program (ACP). The authors acknowledge additional support from the Texas A&M University Supercomputing Facilities and the use of the Laboratory for Molecular Simulations at Texas A&M. We are grateful to R. Volkamer for helpful discussions. The reviewers provided helpful comments for improving this manuscript.

Supporting Information Available: The structural parameters for all the species investigated in this study, selected moments of inertia, frequencies, and mechanistic schemes (PDF). This material is available free of charge via the Internet at http://pubs.acs.org.

JA0350280